Representing Multiple Scales in the Hurricane Weather Research and Forecasting Modeling System: Design of Multiple Sets of Movable Multilevel Nesting and the Basin-Scale HWRF Forecast Application

XUEJIN ZHANG,[a,b] SUNDARARAMAN G. GOPALAKRISHNAN,[b] SAMUEL TRAHAN,[c,d] THIAGO S. QUIRINO,[b] QINGFU LIU,[d] ZHAN ZHANG,[c,d] GHASSAN ALAKA,[a,b] AND VIJAY TALLAPRAGADA[d]

[a] *Cooperative Institute for Marine and Atmospheric Studies, University of Miami, Miami, Florida*
[b] *AOML/Hurricane Research Division, Miami, Florida*
[c] *I.M. Systems Group, Inc., Washington, D.C.*
[d] *NCEP/Environmental Modeling Center, Washington, D.C.*

(Manuscript received 9 May 2016, in final form 3 October 2016)

ABSTRACT

In this study, the design of movable multilevel nesting (MMLN) in the Hurricane Weather Research and Forecasting (HWRF) modeling system is documented. The configuration of a new experimental HWRF system with a much larger horizontal outer domain and multiple sets of MMLN, referred to as the ''basin scale'' HWRF, is also described. The performance of this new system is applied for various difficult forecast scenarios such as 1) simulating multiple storms [i.e., Hurricanes Earl (2010), Danielle (2010), and Frank (2010)] and 2) forecasting tropical cyclone (TC) to extratropical cyclone transitions, specifically Hurricane Sandy (2012). Verification of track forecasts for the 2011–14 Atlantic and eastern Pacific hurricane seasons demonstrates that the basin-scale HWRF produces similar overall results to the 2014 operational HWRF, the best operational HWRF at the same resolution. In the Atlantic, intensity forecasts for the basin-scale HWRF were notably worse than for the 2014 operational HWRF, but this deficiency was shown to be from poor intensity forecasts for Hurricane Leslie (2012) associated with the lack of ocean coupling in the basin-scale HWRF. With Leslie removed, the intensity forecast errors were equivalent. The basin-scale HWRF is capable of predicting multiple TCs simultaneously, allowing more realistic storm-to-storm interactions. Even though the basin-scale HWRF produced results only comparable to the regular operational HWRF at this stage, this configuration paves a promising pathway toward operations.

1. Introduction

Tropical cyclones (TCs) are intense atmospheric circulations initiated by a variety of phenomena, such as easterly waves, monsoon troughs, and even frontal boundaries. Broadly, a TC consists of an inner core, which includes the eye and eyewall for more intense cases, and spiral rainbands, which extend hundreds of kilometers outward from the inner core. Mature TCs are characterized by multiscale interactions with the synoptic-scale environment in which they are embedded. Since a TC may propagate up to thousands of kilometers from genesis to dissipation, the evolution of the synoptic-scale environment throughout a TC life cycle is crucial to accurately predicting multiscale interactions and, consequently, to reducing TC track and intensity errors.

To forecast such complicated phenomena, a regional or global prediction system, especially one that is capable of resolving convective cloud systems at 1–3-km horizontal resolution, is indispensable. However, because of current stringent operational requirements and limited computational resources, it is not viable to operate such a forecast system at a uniform 1–3-km resolution. For more than three decades, scientists have contrived numerical models with movable nested high-resolution meshes or more complicated adaptive meshes (e.g., Kurihara et al. 1979; Liu et al. 1997; Wang 2001; Gopalakrishnan et al. 2002) to effectively simulate/forecast TC systems without compromising scientific requirements. In the early 2000s, the development of an operational TC forecast system with a nonhydrostatic dynamic core was initiated at the National Oceanic and

Corresponding author e-mail: Dr. Xuejin Zhang, xuejin.zhang@noaa.gov

DOI: 10.1175/WAF-D-16-0087.1

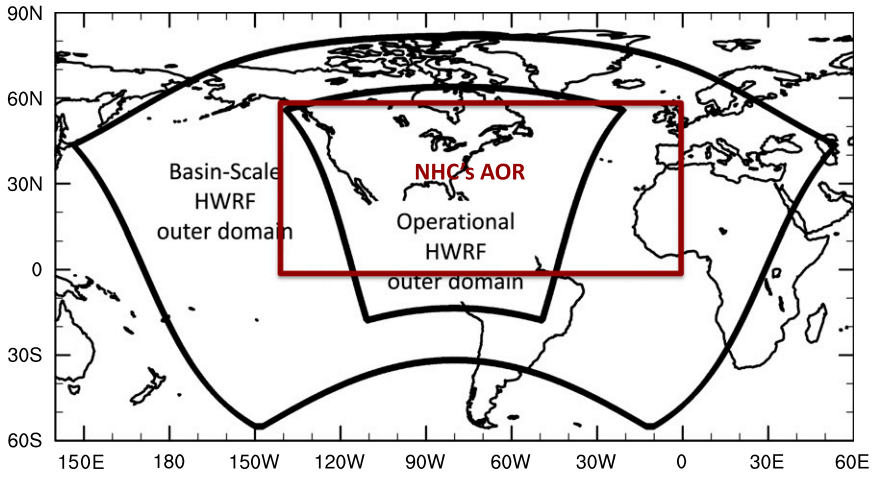

FIG. 1. Schematic domains of basin-scale HWRF, operational HWRF, and NHC's areas of responsibility (AOR).

Atmospheric Administration's (NOAA) National Centers for Environmental Prediction/Environmental Modeling Center (NCEP/EMC) to more accurately forecast TC intensity, structure, and rapid intensity changes.

The Hurricane Weather Research and Forecasting (HWRF) modeling system began running operationally at NCEP in 2007 to provide the National Hurricane Center (NHC) with operational track and intensity forecast guidance. Initial implementation of the HWRF model consisted of a resolution of 27 km for the static domain and 9 km for the single movable nest. Scientists at the Atlantic Oceanographic and Meteorological Laboratory's Hurricane Research Division (HRD) developed an experimental research version of HWRF (HWRFx; Zhang et al. 2011) to target the intensity change problem. They developed a new nesting algorithm within HWRFx and demonstrated its potential to improve TC intensity forecasts (Zhang et al. 2011; Gopalakrishnan et al. 2011). HWRFx was utilized to run retrospective forecasts in the Atlantic basin (Zhang et al. 2011; Gopalakrishnan et al. 2012; Yeh et al. 2012; Pattanayak et al. 2012) and idealized cases (Gopalakrishnan et al. 2011; Bao et al. 2012; Gopalakrishnan et al. 2013). Based on these developments and with the support of NOAA's Hurricane Forecast Improvement Project (HFIP), the first-ever operational TC forecast system with convection-permitting resolution was transitioned into operations in 2012 (Tallapragada et al. 2014; Goldenberg et al. 2015). The forecast system incorporated a movable multilevel nesting (MMLN) algorithm with planetary boundary layer (PBL) and surface physics carefully calibrated using available in situ observations obtained from the hurricane inner-core region (Gopalakrishnan et al. 2013) and an improved vortex initialization scheme documented in the online HWRF scientific documentation.[1] The development of the MMLN will be described later in this paper.

Tallapragada et al. (2014) documented the 2012 implementation of the HWRF system and its performance during the 2010–11 hurricane seasons. Their verifications showed that the 5-day track and intensity forecast errors were reduced by about ~19% and 7% for the North Atlantic basin and by ~9% and 30% for the east Pacific basin, respectively, compared with the previous operational versions of HWRF. Verification of storm size also indicated a dramatic improvement in terms of wind radii at 17.5 m s^{-1} (34 kt), 25.7 m s^{-1} (50 kt), and 32.9 m s^{-1} (64 kt) in each quadrant at all forecast lead times. The overestimation of storm size in the previous operational HWRF system was alleviated at all forecast lead times. Tallapragada et al. (2014) attributed the improved forecasts to some important implementations: 1) the new, higher-horizontal-resolution (3 km) nest that better resolves convection and represents terrain effects, 2) PBL and surface physics for the higher-resolution nest, and 3) improved representation of the initial conditions in the higher-resolution nest. To improve the intensity forecasts even more, several important additional modifications, such as increasing the frequency of physics calls and better vortex initialization, were implemented in the 2013 operational version of HWRF, resulting in significant reductions in intensity forecast errors and even further reductions in track forecast errors (Goldenberg et al. 2015).

[1] The online HWRF scientific documentation is annually updated along with a latest release of the HWRF code. The latest version is available online (http://www.dtcenter.org/HurrWRF/users/docs/scientific_documents/HWRF_v3.7a_SD.pdf).

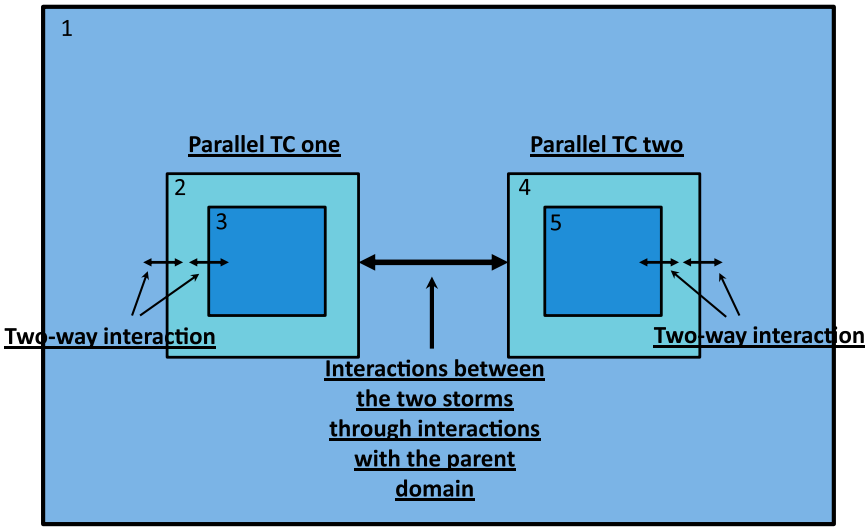

FIG. 2. Schematic interactions between parent-and-child domains in the HWRF-B system with multiple sets of MMLN.

Although the operational HWRF system represents a significant advancement in TC forecasts (i.e., track, intensity, and structure), several deficiencies remain that limit its accuracy and potential for further improvements. The operational HWRF system is configured as follows: 1) the static (i.e., not moving during a given forecast) outer-domain center is located either within ~5° northwest of the TC center or at 35°N if the TC center is north of that latitude and 2) the centers of the movable intermediate and innermost domains are collocated at the TC location prescribed by NCEP. This TC-centric configuration results in an outermost domain that covers only a portion of the particular basin (e.g., North Atlantic or east Pacific hurricane basins) and nearby landmasses. The TC environment and inner-domain boundaries are assumed to be adequately represented for short-range forecasts for each TC. The outermost domain has to be repositioned at the start of each forecast cycle according to the latest initial TC location. This repositioning of the outermost domain may lead to several deficiencies in the cycling forecast system. First, the underlying surface forcings may be dramatically altered; for example, for a TC in the Atlantic, the Rocky Mountains may be located within the domain in one forecast cycle but not in a subsequent or prior cycle. Second, this can also cause model initialization and physical processes to be inconsistent from cycle to cycle. And third, the environmental flow and lateral boundaries may become inconsistent from cycle to cycle in track prediction because of location changes of the operational domain. To alleviate these potential model configuration deficiencies, we developed an HWRF system with an outer domain that is large enough horizontally to remain static (fixed) from forecast to forecast (Fig. 1). In the case of the model configuration designed for TC forecasts in the Atlantic and east Pacific, the outer domain encompasses both of these basins. In addition, this larger domain allows for multiple sets of MMLN within the static outermost domain to allow for simultaneous forecasts of several TCs within one model run, whereas current operational configuration of HWRF has to be run separately for each TC present at the initial forecast time since it has only a single set of MMLN. The system can forecast a single

TABLE 1. Three major components of the HWRF-B forecast system.

Initialization	Forecast system	Products and dissemination
Static terrestrial initialization	Trigger mechanism	Vortex- and large-scale postprocessing
Initialization and cycling	Resource allocation	Diagnostic and forecast products
Vortex initialization (relocation and modification)	Submission and monitor system (jobs and resource management)	Web products
Data assimilation		Product real-time dissemination
		Tape archive
		Gridded binary (GRIB) file generation

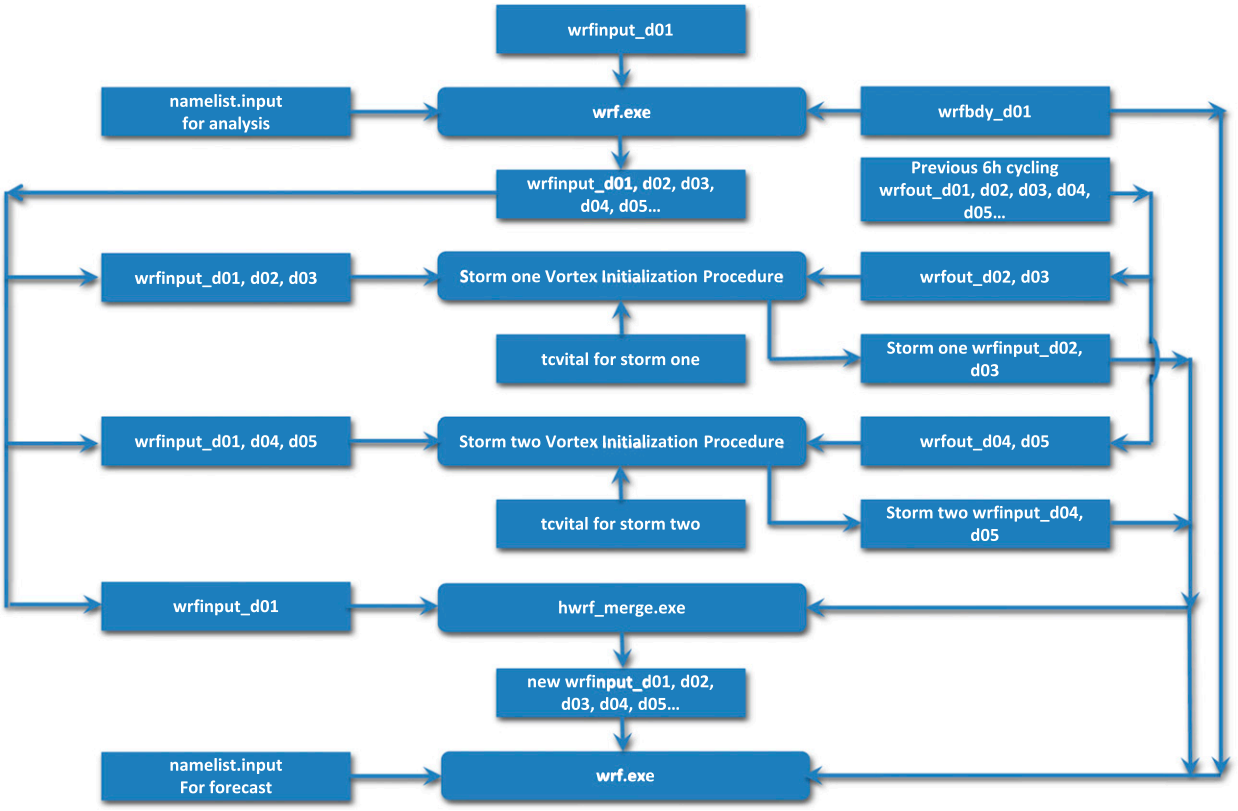

FIG. 3. Flowchart for the MMLN vortex initialization implementation in the HWRF-B. We use wrfinput_d0[1,2,3,4,5] to represent the input files for the respective domains at the initial time and wrfout_d0[1,2,3,4,5] for the output files. The outermost domain is d01, d0[2,4] are the intermediate domains, and d0[3,5] are the innermost domains. To define the TC initial parameters, a tcvital file is provided by NHC. To configure the model, a namelist.input file is used. The final analysis of the outmost domain is generated by hwrf_merge and wrf.exe is the model executable.

solution for the large-scale environment and solutions for multiple TCs concurrently from one cycle to another if more than one TC is present in the basin-scale HWRF domain.

We document the details of constructing the multiple sets of MMLN in the basin-scale HWRF (hereafter HWRF-B) system in section 2. We briefly describe the HWRF-B modeling system and its initialization procedure in section 3, and the model configuration, experimental design, and the major physics schemes in section 4. In section 5, using the HWRF-B modeling system, we show an example of a multistorm forecast for Hurricanes Earl, Danielle, and Frank (2010); the single-storm forecasts for Hurricane Sandy (2012); and also verify retrospective and real-time forecasts for four hurricane seasons (2011–14). Our conclusions appear in section 6. To fully present the multiple sets of MMLN in the HWRF-B, several aspects of the MMLN in the 2012 operational HWRF version, the first operational version to implement the MMLN, will be documented in the appendix.

2. Design of the multiple sets of MMLN

HWRF is a variant of the WRF Nonhydrostatic Mesoscale Model (WRF-NMM; Janjić et al. 2001), with a movable-nest capability and physics schemes suitable for TC predictions (Gopalakrishnan et al. 2006; Gopalakrishnan et al. 2012). The system is embedded within the WRF software framework (Michalakes et al. 2004). The major advancement in the high-resolution HWRF system is the MMLN. The concise algorithm of MMLN in the operational HWRF is documented in the appendix. For details on the algorithm and its updates, readers can refer to the online HWRF scientific documentation.[2]

The HWRF-B system is configured with multiple sets of MMLN (Fig. 2). The large arrows in Fig. 2 indicate the interactions between the two TC entities. We make an assumption that interactions are implicitly reflected

[2] See footnote 1.

TABLE 2. Operational and basin-scale HWRF configurations. The operational HWRF system is changed every year. The operational HWRF configurations in 2011 and 2012 were documented in Tallapragada et al. (2014).

	2013 operational HWRF (H213)	2013 basin-scale HWRF (H3HW)	2014 operational HWRF (H214)
Domain	27 km: 77.58° × 77.58° 9 km: 10.56° × 10.2° 3 km: 6.12° × 5.42°	27 km: 178.20° × 77.58° 9 km: 10.56° × 10.2° 3 km: 6.12° × 5.42°	27 km: 77.58° × 77.58° 9 km: 12.66° × 12.18° 3 km: 7.90° × 7.06°
Vertical levels	43	61	61
Model top	50 hPa	2 hPa	2 hPa
Vortex initialization	Modified vortex initialization at 3 km, with a 30° × 30° analysis domain and GSI	27 km: GFS 9–3 km: no, downscaled	Improved vortex initialization Improved GSI DA
Cycling	Yes (3-km vortex only)	Same as H213	Same as H213
Ocean coupling	27–9 km: yes 3 km: no, downscaled	Static SST	Same as H213
	Physics schemes		
Microphysics	Modified Ferrier (high resolution)	Same as H213	Modified H213
Radiation	GFDL	Same as H213	Same as H213
Surface	GFDL (high resolution)	Same as H213	Same as H213
PBL scheme	2013 GFS (high resolution)	Same as H213	Same as H213 with modified K_m
Convection	SAS (high resolution), no convective parameterization (3 km), shallow convection	Same as H213	Same as H213 with improved SAS
Land surface	GFDL slab	Same as H213	Same as H213

through child-to-parent/parent-to-child feedbacks among individual TCs when multiple sets of MMLN are not overlapped. The dynamic and physical processes during TC interactions happen through a linkage of environmental systems around the TCs. Thus, this assumption simulates the real interactions among TCs through contributing fluxes and momentum to the TC environment. The direct interactions occur when two sets of MMLN overlap, meaning both MMLN solutions will feed back to the parent solutions in the same time step. We apply the above approach of interactions between multiple storms because the interactions physically occur through the ambient environment (Xu et al. 2013). The effect of one TC on neighboring TCs can be conveyed through feedback on the circulation and thermal fields in the parent domain.

The approach is also part of a parallel-computing algorithm, which was independently implemented with Portable Operating System Interface (POSIX) Threads (PThreads) and Message Passing Interface (MPI) programming in the current supercomputer architecture (e.g., Michalakes et al. 2004; Quirino et al. 2014) and will be available in the 2016 release. The strategy of parallelizing the computing for each storm greatly improves the computational performance across massive parallel supercomputer architectures.

3. HWRF-B system

To realize forecasts with multiple sets of MMLN in a real-time forecast system, we developed the HWRF-B automation system at the Hurricane Research Division of NOAA's Atlantic Oceanographic and Meteorological Laboratory (AOML) with partners at EMC and NOAA's Developmental Testbed Center (DTC). The system consists of three major modules: initialization, a forecast system, and products/dissemination (Table 1). During a hurricane season, the modeling system constantly incorporates TC and/or potential TC (i.e., "invests") systems requested by NHC to produce model forecasts through an automatic triggering system. The configuration of the forecast system (e.g., the number of sets of MMLN, etc.) is thereafter determined by the triggering system. The initialization module sequentially processes the static terrestrial initialization, meteorological initialization, and cycling for each TC (and invest) in the domain. The vortex circulation and thermodynamic variables are relocated and rebalanced according to the observed TC surface parameters supplied by operational centers as the operational HWRF does for a single storm. The critical information for vortex initialization includes the center position, intensity (maximum 1-min sustained winds), and structure (radius of 17.5 m s^{-1} winds). The HWRF-B may be configured with up to nine sets of MMLN. However, the available computational resources on the JET[3]

[3] The JET supercomputer is a NOAA research and development supercomputer system used for HFIP demo forecasts during the hurricane season.

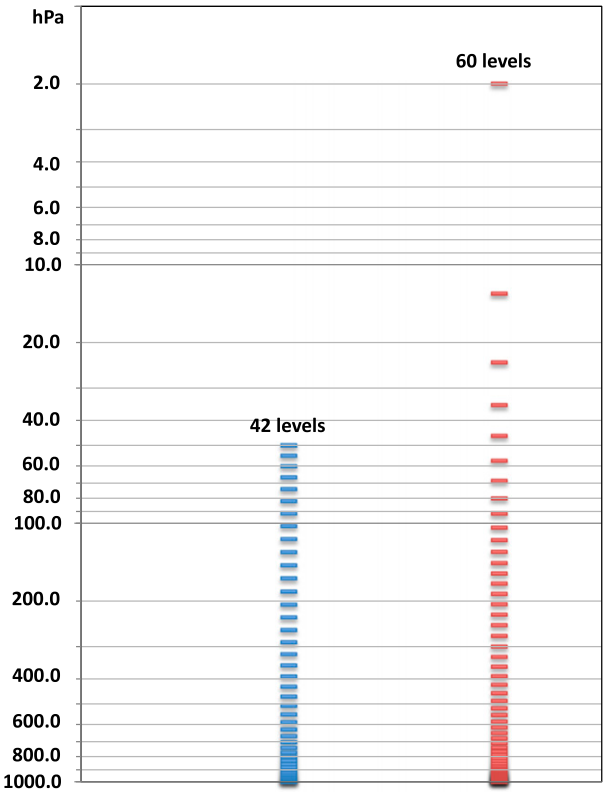

FIG. 4. Vertical hybrid coordinates in the 2013 operational HWRF, the 2014 operational HWRF, and the HWRF-B modeling systems. Blue bars (from 2013 operational HWRF) represent the sigma levels with surface pressure at 1013 hPa and model top at 50 hPa, and red bars (from the 2014 operational HWRF and HWRF-B) are for the same surface pressure and model top at 2 hPa.

supercomputer allow us to concurrently forecast only up to four TCs/invests in the HWRF-B modeling system in the semi-real-time mode.

As with the operational HWRF system, the generation of initial conditions for the prognostic variables in the nests is an important component of the HWRF-B system. In the same way as the operational HWRF system, with the exception of topography and prognostic variables (e.g., horizontal winds, temperature, moisture, and mass), all other terrestrial variables of the individual nests are initialized by the corresponding variables in the parent domain. The respective resolutions of topography for different level nests in the entire outermost domain are generated during the preprocessing stage. During the initialization of the geopotential height, temperature, and moisture fields, the hydrostatic approximation is assumed. In the HWRF-B modeling system, after we first initialize each set of MMLN as is done in the operational HWRF system, we then merge all sets of MMLN and generate the initial conditions for the HWRF-B. Figure 3 shows the flowchart of the vortex initialization implemented in the HWRF-B forecast system for multiple sets of MMLN. In the first forecast cycle for a TC, a synthetic votex[4] is implanted into the position based on the observed TC parameters. After the first forecast, each subsequent forecast cycles the TC vortex from the previous 6-h forecast. The steps in the vortex initialization procedure are the same as in the operational HWRF system. However, if multiple TCs are present, the TC vortices are removed from the environmental fields and rebalanced one by one (Kurihara et al. 1998). After completing the above procedure, the rebalanced cycled vortex is placed in the vortex-removed GFS environmental fields at the observed position to produce the final analysis of the initial conditions. If multiple TCs exist, the initialization procedure is repeated for each TC concurrently, and each vortex is implanted at the respective observed positions. Similar to the vortex initialization procedure of Kurihara et al. (1998), the environmental fields from the GFS analysis remain intact outside each vortex-filtered domain. The final initial conditions are generated by merging each TC's final analysis. Details are discussed in the online HWRF scientific document.[5] The current initialization has been implemented in operational and research models globally and has provided a practical solution to the vortex initialization problem in mesoscale models since the 1990s (e.g., Wang 1995; Kurihara et al. 1998; Zhao et al. 2007; Hendricks et al. 2011; Tallapragada et al. 2014).

4. Model configuration and design of experiments

The operational HWRF system[6] was used as the benchmark (i.e., baseline) of our study. Table 2 provides the similarities and differences among the 2013 and 2014 operational HWRF systems (H213 and H214, respectively) and the 2013 HWRF-B system (H3HW). The operational HWRF for 2012–14 are configured with an outermost mesh of 0.18° (equivalent to ~27 km along the equator[7]) with the horizontal grid spacing covering 77.58° × 77.58° and one set of MMLN at 0.06° (equivalent to ~9 km) for an intermediate domain and 0.02°

[4] The synthetic vortex is only used for the first cycle and only if the initial intensity is $\geq 14\ \mathrm{m\ s^{-1}}$.

[5] See footnote 1.

[6] This is really a "combination" HWRF since it consists of four different versions; that is, a different operational HWRF version ran during the hurricane season in each of the four years (i.e., H211, H212, H213, and H214), but these are all simply called HWRF in the Automated Tropical Cyclone Forecast (ATCF) A-Deck files.

[7] The actual resolution is the shortest distance between two adjacent grid points where variables are stored, which in the case of the E grid is along a diagonal of the horizontal grid spacings of 0.18°. In the equatorial area, the resolution is around ~27 km.

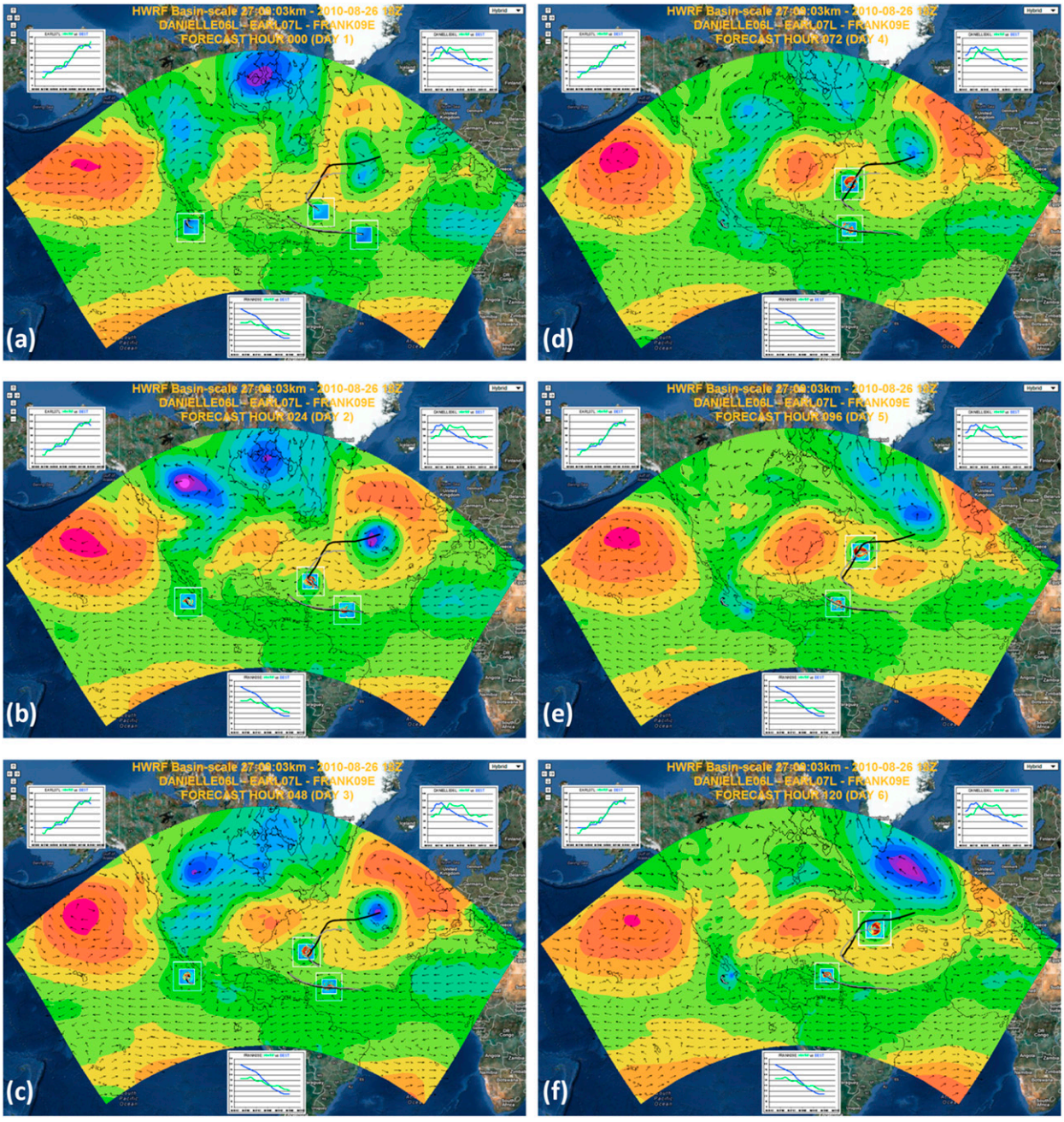

FIG. 5. Real-time, 3-km forecasts of Hurricanes Earl, Danielle, and Frank at 1800 UTC 26 Aug 2010 for (a) 0, (b) 24, (c) 48, (d) 72, (e) 96, and (f) 120 h. The inset panels show the intensity forecasts of Hurricanes Earl (top left) and Danielle (top right) in the Atlantic basin, and Frank in the east Pacific (bottom middle). Earl is to the left, Danielle in the middle, and Frank to the right at the initial time.

(equivalent to ~3 km) for an innermost domain (see details in Table 2). The 2011 operational HWRF version does not have the ~3-km innermost mesh (Goldenberg et al. 2015). There are 42 hybrid levels with 10 levels below 850 hPa and the model top at 50 hPa in the 2013 and earlier versions of operational HWRF, and 61 hybrid levels with 21 levels below 850 hPa and the model top at 2 hPa in the 2014 version of the operational HWRF. In the HWRF-B, the model is configured with an outermost mesh of 0.18° and horizontal grid spacing covering 178.20° × 77.58° and with the same size domains for each set of MMLN as in the operational system. There are 61 hybrid levels with 21 levels below 850 hPa and the model top at 2 hPa in the HWRF-B

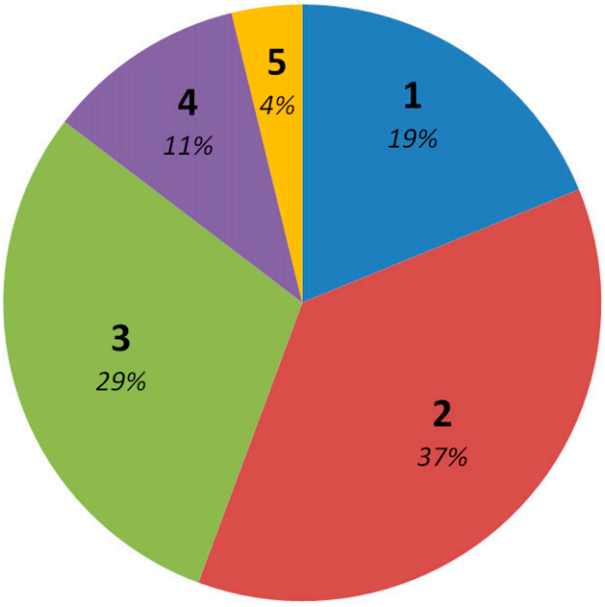

FIG. 6. Frequency statistics of multiple TCs in the Atlantic and east Pacific basins during the 2011–14 hurricane seasons when there is at least one verifiable TC in the Atlantic basin at the initial time. At least one additional TC (including invest storms) is found for 81% of the cycles and 44% of cycles have at least two more additional TCs at the verified time.

system as in the 2014 version of the operational HWRF (Fig. 4). The main upgrade to the 2013 operational HWRF for the 2014 version is this increase in vertical levels. Therefore, for the purposes of verification in section 5, the 2014 operational HWRF (H214) is the version that is expected be the closest to the HWRF-B version (H3HW). Other than the basic differences inherent in the basin-scale design (larger horizontal domain of outer static mesh and ability for multiple sets of MMLN), the only substantial difference in the model implementation between H214 and H3HW is that H214 is coupled to the ocean model, whereas H3HW is not.

The model physics used in HWRF-B in this study were configured as closely as possible to the operational HWRF system. An extensive overview of the physics schemes used in the HWRF systems is provided in Gopalakrishnan et al. (2011), Yeh et al. (2012), and the online HWRF scientific documentation.[8] The Ferrier scheme (Ferrier 2005) was used to provide latent heating due to the microphysical processes in the atmosphere, and the simplified Arakawa–Schubert scheme, known as the SAS scheme (Pan and Wu 1995; Hong and Pan 1998), was used to parameterize subgrid cumulus cloud activity. The SAS scheme in combination with microphysical parameterization was used for both the outermost and intermediate domains, while it was deactivated in the innermost domain. The Geophysical Fluid Dynamics Laboratory's (GFDL) longwave radiation transfer scheme that follows the simplified exchange method of Fels and Schwarzkopf (1975) and Schwarzkopf and Fels (1991) and the shortwave radiation transfer scheme of Lacis and Hansen (1974) were also used in the current study.

The HWRF system uses the GFDL surface-layer parameterization scheme (Sirutis and Miyakoda 1990; Kurihara and Tuleya 1974). The parameters were calibrated from the most recent laboratory experiments (Haus et al. 2010) and field experiments (Zhang et al. 2008; Montgomery et al. 2012; Gopalakrishnan et al. 2013), while the drag coefficient C_k, computed in the HWRF system, was modified to fit the observed estimates for both weak and strong regimes since 2012 (Gopalakrishnan et al. 2013). With these upgrades to the surface-layer scheme, the HWRF system provides a reasonable surface flux exchange within the range of observational uncertainties. The modified GFS boundary layer formulation (Hong and Pan 1996; Gopalakrishnan et al. 2013) is used to parameterize the flux transport and subsequent mixing in the atmosphere according to the synthesis observations since 2012 (Zhang et al. 2011a,b).

5. Results and discussion

a. *Multiple-TC forecasts with multiple sets of MMLN*

Figure 5 shows an example from a real-time forecast of HWRF-B with multiple sets of MMLN (i.e., H3HW). The boxes illustrate three TCs: Hurricane Earl (2010) and Hurricane Danielle (2010) in the Atlantic basin and Hurricane Frank (2010) in the east Pacific basin concurrently initialized at 1800 UTC 26 August 2010. The black and gray lines denote actual tracks (a.k.a. best tracks) determined by NHC and the forecast tracks predicted by the basin-scale modeling system, respectively. The example demonstrates that the new capability of multiple sets of MMLN in the HWRF-B modeling system is numerically and dynamically feasible for real-time TC forecasting.

Concurrent TCs in the Atlantic and east Pacific basins are quite common. As shown in the frequency statistics in Fig. 6, 81% of forecast cycles with a verifiable TC in the Atlantic basin during the 2011–14 hurricane seasons have at least one additional TC or invest at the initial time. It is also impressive that 44% of cycles have at least two additional TCs. With the new capability of the HWRF-B modeling system to use multiple sets of MMLN, the large-scale environment for multiple TCs/vortices should be forecast within the same basin-scale

[8] See footnote 1.

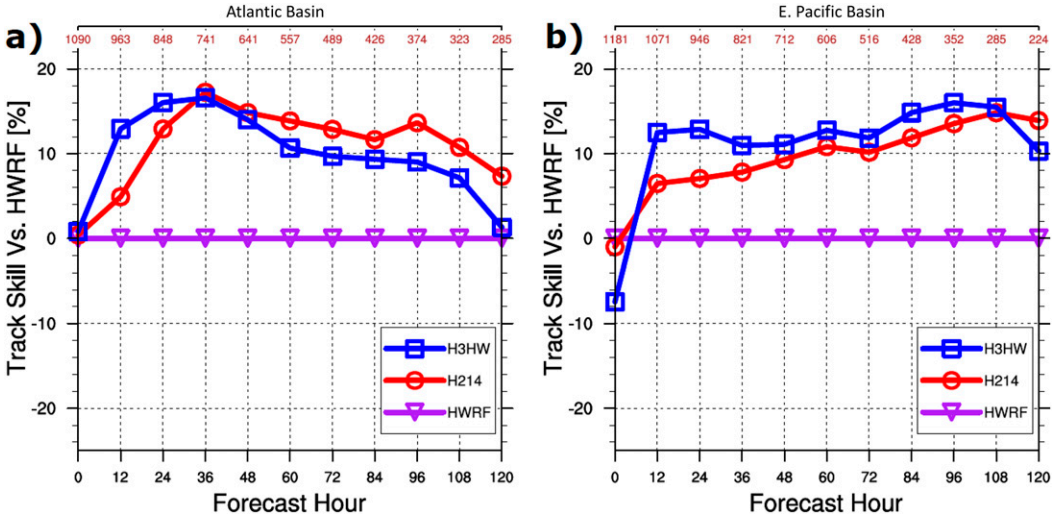

FIG. 7. Track verification for (a) Atlantic and (b) east Pacific basin TCs during the 2011–14 hurricane seasons. H3HW is the HWRF-B (blue line), H214 is the 2014 operational HWRF (red line), and HWRF is a combination of the various versions of the operational HWRF (purple line) during 2011–14. The track skills are defined as the skill vs the combination operational HWRF.

domain. The cycling of the single environment and multiple TCs/vortices are immediately available to further data assimilation (e.g., Ngodock et al. 2007; Hsiao et al. 2012). This implementation will also provide a new paradigm for TC numerical prediction that can be extended to a 7-day forecast in the future.

b. *Verification of track and intensity forecast errors*

Verifications are presented here for the HWRF-B (H3HW) and the 2014 operational HWRF (referred to here as H214) versus the real-time operational HWRF runs (referred to here simply as HWRF) for the 2011–14 Atlantic and east Pacific hurricane seasons.[9] We produced retrospective forecasts for the 2011–12 hurricane seasons and real-time forecasts for the 2013–14 hurricane seasons using H3HW (see Table 2 for configuration) on HFIP's JET computer. The initial conditions and lateral boundary conditions were generated from operational GFS analyses and forecasts during the 2013–14 seasons. The same version of the GFS, including its data assimilation system, was used for the retrospective forecasts of the 2011–12 hurricane seasons. Real-time runs of the H214 were used for the 2014 results and retrospective forecasts using H214 with the same GFS initial and boundary conditions were used for the 2011–13 forecasts.

The percentage improvement of track forecasts from H3HW and H214 over those from the HWRF is represented by a Brier skill score ("skill"). Positive (negative) skill indicates that H3HW or H214 produced better (worse) forecasts than HWRF. Figure 7 shows the track verification for the 2011–14 hurricane seasons.[10] The results for the TCs from the Atlantic hurricane basin (Fig. 7a) show that the H3HW and H214 consistently produced 8%–16% improvements in track forecasts (Fig. 7a; i.e., smaller track errors) than HWRF at all forecast intervals except at 120 h. Figure 7b demonstrates a similar (6%–16%) improvement in the east Pacific basin. However, note that the skill of H3HW and H214 versus the baseline (HWRF) is really only showing that the HWRF model has greatly improved during those several years. The important comparison here is between H3HW and H214, since the primary difference between these two is simply the design of the HWRF-B—larger horizontal domain and multiple sets of MMLN—so this comparison focuses instead on the impact and effectiveness of those basin-scale enhancements. In the Atlantic (Fig. 7a), H3HW is comparable (within ±2%–3%) to H214 and slightly better for more forecast intervals. In the east Pacific, H3HW is better than H214 by 2%–5% for most forecast intervals.

In terms of intensity skill (Fig. 8), H214 produced better intensity forecasts than HWRF at all lead times in

[9] See footnote 6.

[10] This study followed the same guidelines used by NHC in its official verifications, in that a forecast was verified only if a system was a tropical (or subtropical) cyclone (depression intensity or greater) at the initial time and the verification time (Goldenberg et al. 2015).

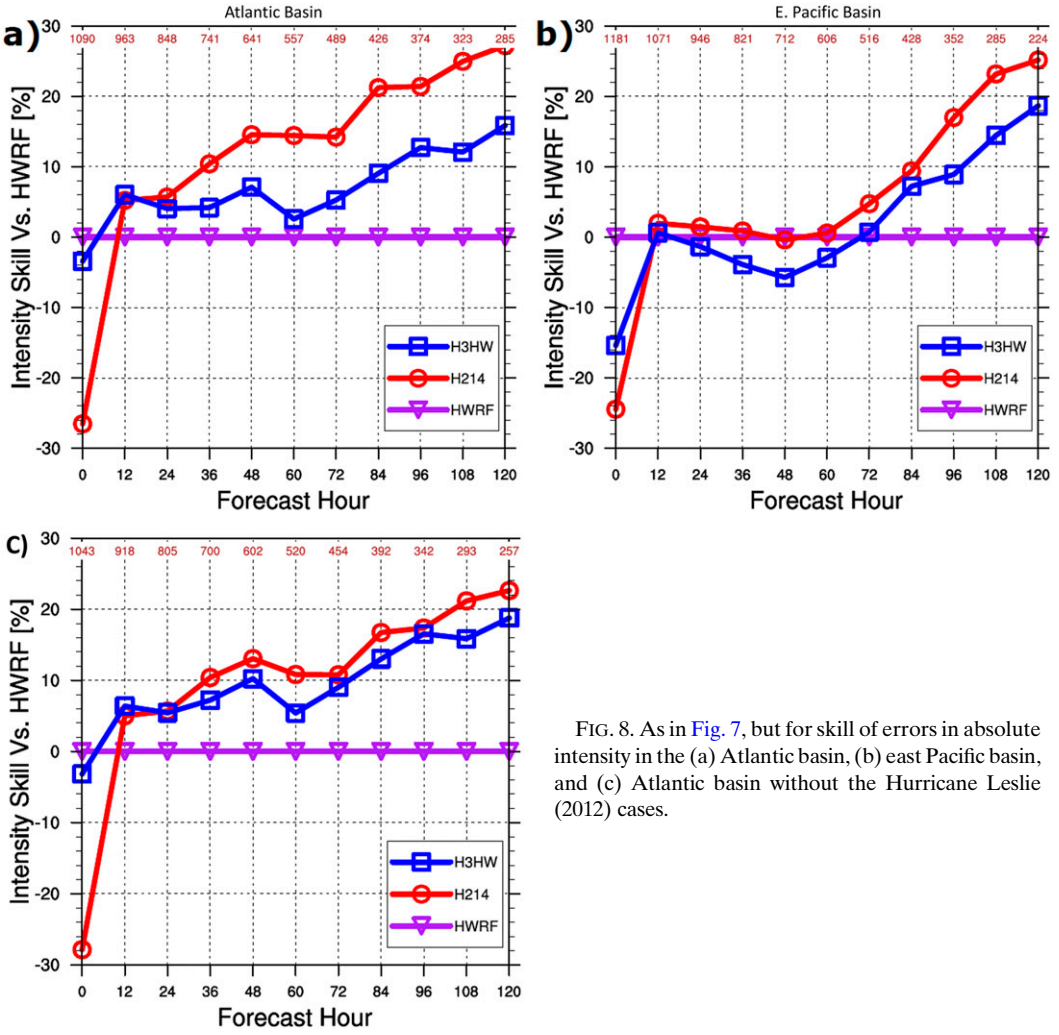

FIG. 8. As in Fig. 7, but for skill of errors in absolute intensity in the (a) Atlantic basin, (b) east Pacific basin, and (c) Atlantic basin without the Hurricane Leslie (2012) cases.

the Atlantic basin and for longer lead times in the east Pacific basin. H3HW had slightly lower skill but was generally very close to H214 in the east Pacific (Fig. 8b). However, the differences are much greater between H3HW in the Atlantic (Fig. 8a). It has been noted that the main difference between the model setup for H3HW and H214 is that H3HW is not yet coupled with the ocean model. The lack of ocean coupling may significantly influence the TC intensity change when the sea surface temperature cannot be represented accurately at the initial time because the real-time retrieval of SST from satellite data has more bias in the cloudy sky (Yablonsky and Ginis 2013). By comparing forecasts from H3HW and H214, we found the large intensity errors mainly came from the slow-moving TCs, such as Hurricane Leslie (2012) in the Atlantic basin and Hurricane Miriam (2012) in the east Pacific basin. Redoing the verifications for the Atlantic without Hurricane Leslie (Fig. 8c) produced substantial improvements in the intensity forecasts for H3HW, especially versus H214. This was in spite of the fact that the Leslie cases accounted for $<10\%$ of the total. This demonstrates how strongly the H3HW Leslie intensity forecasts were hampered by the lack of ocean coupling. In general, we believe coupling the ocean and atmosphere models may be critical to improving intensity forecasts for certain cases, especially for slow-moving TCs in the Atlantic and east Pacific basins.

c. *Hurricane Sandy forecast*

Hurricane Sandy (2012) was a TC that experienced complex interactions with synoptic systems during its life cycle. During the early stages after its formation, Sandy intensified steadily and reached major hurricane strength ($51.4\,\mathrm{m\,s^{-1}}$ at 0525 UTC 25 October 2012) before making landfall in eastern Cuba. After its passage over Cuba, Sandy began interacting with southwesterly

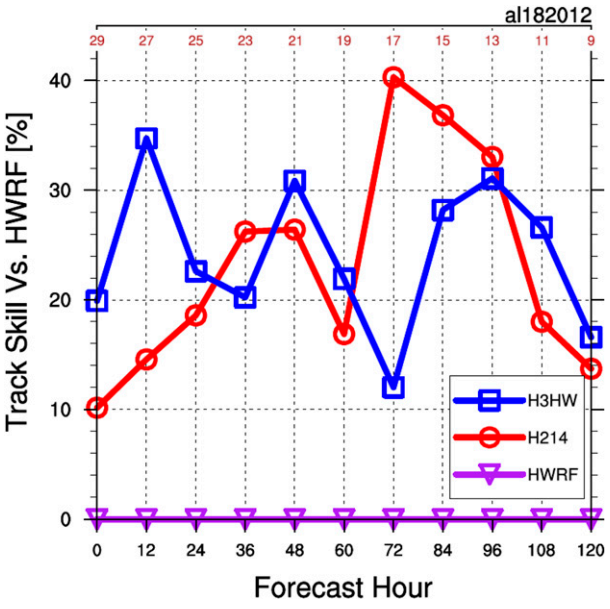

FIG. 9. As in Fig. 7, but for Hurricane Sandy (2012).

shear, an upper-level trough, and a cold, dry air mass (Blake et al. 2013).

Lorenz (1969) points out that subtle forecast errors in environmental flows may result in significant forecast errors within a few days. The H3HW track forecasts showed 10%–40% improvement over the 2012 operational HWRF track forecasts at all lead times, which is consistent with the improvements shown by H214 (Fig. 9). Interestingly, all forecasts were driven by a similar vortex initialization procedure and large-scale GFS fields from the same version of GFS modeling system (see NCEP/EMC implementation website for details[11]). H3HW and H214 both have improved dynamics and physics, but different configurations (Table 2). However, H3HW was able to better capture the environment, which was key to the track predictions of Hurricane Sandy (Shen et al. 2013). These improvements partially contributed to accurate predictions of Sandy's westward bend. Our findings suggest that the subtle differences in forecasts and subsequent multiscale interactions with the evolving synoptic-scale environment surrounding Sandy were important for improved predictions. The 500-hPa geopotential heights are shown for the GFS analysis, H3HW, H214, and the GFS forecast 90 h into a forecast initialized at 1200 UTC 25 October 2015 (Fig. 10). The errors of the last three models relative to the GFS analysis are shaded in Fig. 10. Our analysis indicates that Hurricane Sandy follows the 5550-gpm line moving toward the northwest in the GFS analysis. The steering flow induced by the adjacent synoptic systems, including the blocking high over the North Atlantic, a trough over the central United States, and a small low center in the southeastern United States broken off from the main trough, guided Sandy's sharp westward motion. H3HW accurately predicted the position and amplitude of all three systems and, therefore, the track. We found that neither the H214 nor GFS forecast predicted the separation of the small low in the southeast United States from the main trough axis to its north and neither bent Sandy's track far enough to the west (Figs. 10c,d). The errors suggest that the blocking high and trough positions are the primary factors that impact the westward bend to Sandy's track at this time. In the operational HWRF forecast, the blocking high was too far east and the main trough in the central United States was too weak, both of which resulted in the northeastward motion of Sandy and larger track errors (not shown; refer to the real-time operational HWRF website for details[12]). A detailed investigation of Sandy forecasts in the HWRF-B is a topic for future research.

6. Conclusions

We have developed an experimental HWRF-B modeling system at AOML/HRD in collaboration with NCEP/EMC under the support of NOAA's HFIP. The system can support any number of high-resolution movable nests centered on TCs that exist in either the Atlantic or east Pacific hurricane basins. This system not only provides simultaneous, high-resolution forecasts of multiple TCs, but also has the potential to improve the representation of TC–TC interactions, synoptic-scale circulation, and TC life cycles from genesis to decay. The HWRF-B system may be applied to diagnose model bias, to improve physics schemes, to initialize multiple vortices locally, and to advance regional data assimilation techniques.

Similar to the operational HWRF modeling system, the HWRF-B system consists of three key components: initialization, a forecast system, and a postprocessing/production system. The existing vortex initialization scheme in the HWRF modeling system was extended to the HWRF-B system so that any number of TCs can be seamlessly initialized at the 3-km resolution of the innermost nest. The design of the multiple sets of MMLN,

[11] The GFS modeling system used in this study was implemented at 1200 UTC 22 May 2012. Technical details are available in the date tag: 2012052212 (http://www.emc.ncep.noaa.gov/GFS/impl.php).

[12] Information is available from the operational HWRF real-time forecast website (http://www.emc.ncep.noaa.gov/gc_wmb/vxt/HWRF/tcall.php?selectYear=2012&selectBasin=North%20Atlantic&selectStorm=SANDY18L).

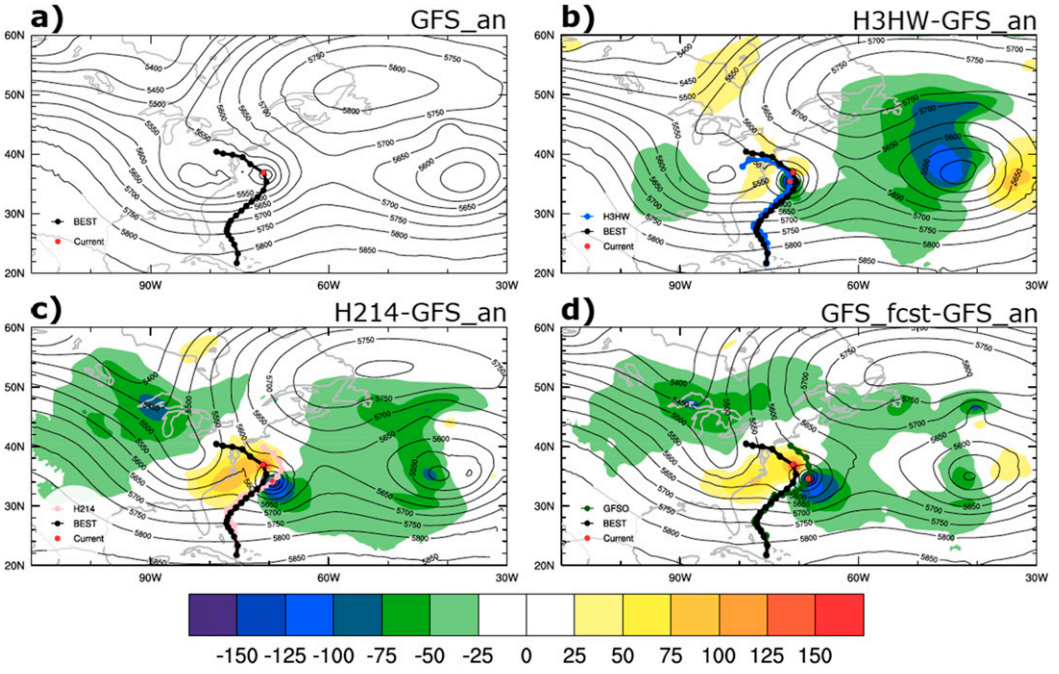

FIG. 10. For the 90-h forecast from an initial time of 1200 UTC 25 Oct 2012, the 500-hPa geopotential heights and their deviations of the HWRF-B, the operational HWRF, and the GFS forecasts vs the GFS analysis overlapped by the best track (black line) and HWRF-B (blue line), the 2014 operational HWRF (pink line), and the operational GFS (green line) forecast tracks. Results are shown for (a) GFS-analyzed geopotential heights and the best track of Sandy, (b) the deviation and HWRF-B, (c) the 2014 version of the operational HWRF, and (d) the real-time GFS. The contours are the geopotential heights and shaded colors are the deviations.

their feedbacks, and interactions have taken into account operational requirements for concurrent model forecast integrations that can be produced for any number of TCs in the region. The design can be further applied to the next-generation, multiscale regional or global modeling system for hurricane forecasting.

Using the HWRF-B system, we have verified the forecasts for four hurricane seasons (2011–14) in the Atlantic and east Pacific basins, in particular comparing the HWRF-B (H3HW) and the 2014 operational HWRF (H214), since these two versions of HWRF are roughly the same with the exception of the core modifications for the basin-scale version: a larger horizontal domain and multiple sets of MMLN. Also, H3HW did not use ocean coupling. Other than poor intensity forecasts for Hurricane Leslie with H3HW (shown to be due to the lack of ocean coupling) compared with H214, the track and intensity forecasts for these two models were similar. Although one would have hoped that H3HW would have produced at least consistently superior track forecasts, there is still an advantage to the basin-scale version in that the forecasts for all of the various TCs can be performed in one run instead of separately. Also, H3HW holds the potential to better capture various types of multi-TC interactions. As a result of a lack of ocean coupling in H3HW and other more minor differences between H3HW and H214, in addition to the basic basin-scale differences, this was not a ''pure'' comparison. Therefore, HRD is currently performing controlled tests using the 2015 versions of the basin-scale and operational HWRF versions, where the *only* differences are the basic enhancements that comprise the basin-scale version. These results will be presented in a future publication.

We further demonstrated that HWRF-B reduced track errors and improved the landfall forecast in the case of Hurricane Sandy (2012) because of more accurate forecasting of the synoptic-scale and/or planetary-scale evolution, which steered Hurricane Sandy more westward even though both the operational HWRF and HWRF-B systems were forced by the same large-scale GFS forecast. The superiority of the basin-scale HRWF forecasts of Sandy suggests the need for a transition from a storm-centric to a basin-centric system and eventually a global- to local-scale forecast system for hurricanes.

Finally, we demonstrated the general performance of the HWRF-B system that can concurrently accommodate multiple TCs with MMLN. By using this system, we can study the TC dynamics and physical processes,

improve the high-resolution model physics, identify model deficiencies, and evaluate the localized vortex initialization and data assimilation. The system can also serve as an experimental tool for developing the next-generation of global-to-local-scale TC forecast models.

Acknowledgments. This work is supported by NOAA Awards NA12NWS4680007, NA13OAR4830232, NA14OAR4830119, and HFIP. We thank our colleagues: Stanley Goldenberg and Drs. Sim Aberson and Steve Diaz for their thoughtful comments that improved the manuscripts. We are also grateful to Gail Derr for her detailed editorial comments.

APPENDIX

The HWRF nesting algorithm

As early as the 1920s, scientists began to study the interactions between TCs (Fujiwhara 1921). Based on observational analysis, Lander and Holland (1993) found that all multiple-vortex interactions could be broken down into a generic mode of binary interaction. As seen in Fig. 6, in the vast majority of times when there is a forecast run for a TC, there is at least one other TC or invest in the Atlantic or east Pacific. Such frequent occurrences of multiple storms motivated us to develop a system that could simulate multiple storms at the same time and their direct interaction—the Fujiwhara effect, which is also referred to as binary interaction (Brand 1970). As we have noticed in our further analysis, in many cases the additional storm(s) can be in another basin or outside the operational HWRF domain, then indirect interactions will occur. Before we developed our system of multiple sets of MMLN, we first developed the single-storm MMLN that is currently used in the operational HWRF, which has shown steady improvement after the transition from research to operations. This appendix briefly introduces the key elements of the HWRF nesting algorithm. The nesting algorithm is also applied in the basin-scale system.

a. Grid structure and downscaling interpolation

HWRF is formulated on a rotated latitude–longitude Arakawa E grid along the horizontal direction, with a vertical pressure–sigma hybrid coordinate system. The rotated coordinate is transformed in such a way that the coordinate origin is located at the center of the outermost domain, and the x and y axes are aligned with the new coordinate equator and prime meridian through the domain center, respectively. Nests follow the same grid structure. Subsequently, the nested domains can be moved anywhere within the parent domain.

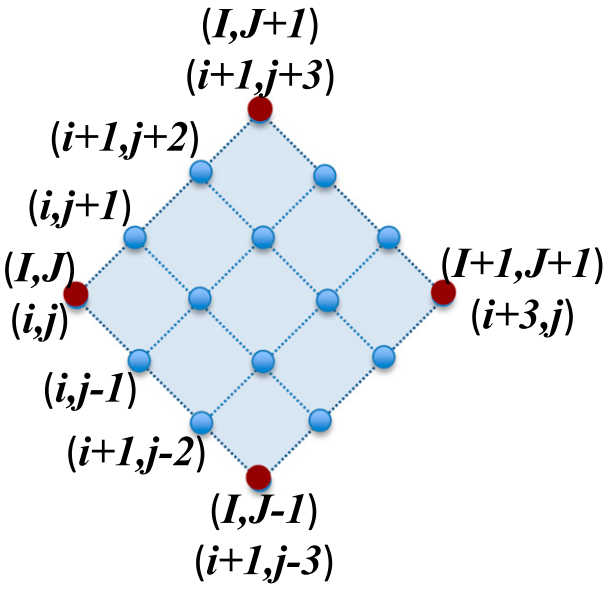

FIG. A1. The schematic E-grid refinement diamond consists of four red dots from the coarse resolution that are used by the bilinear interpolation scheme.

Interpolation from the parent domain to the nested domains is achieved along a rotated latitude–longitude coordinate through bilinear interpolation:

$$\mathbf{A}_{i,j} = b_{I,J}\mathbf{E}_{I,J} + b_{I,J+1}\mathbf{E}_{I,J+1} + b_{I,J-1}\mathbf{E}_{I,J-1} + b_{I+1,J+1}\mathbf{E}_{I+1,J+1}.$$

Here, $\mathbf{A}_{i,j}$ is the prognostic variable matrix on the fine grids, as illustrated in Fig. A1, where $\mathbf{A}_{i,j} = \begin{bmatrix} a_{i,j} & a_{i,j+1} & a_{i+1,j+2} & a_{i+1,j+3} \\ a_{i,j-1} & a_{i+1,j} & a_{i+1,j+1} & a_{i+2,j+2} \\ a_{i+1,j-2} & a_{i+1,j-1} & a_{i+2,j} & a_{i+2,j+1} \\ a_{i+1,j-3} & a_{i+2,j-2} & a_{i+2,j-1} & a_{i+3,j} \end{bmatrix}$, $a_{i,j}$ is the individual element of the matrix, and $b_{I,J}$ is the variable on the coarse grids. The coefficient matrices are defined as

$$\mathbf{E}_{I,J} = \begin{bmatrix} e_{i,j} & e_{i,j+1} & e_{i+1,j+2} & e_{i+1,j+3} \\ e_{i,j-1} & e_{i+1,j} & e_{i+1,j+1} & e_{i+2,j+2} \\ e_{i+1,j-2} & e_{i+1,j-1} & e_{i+2,j} & e_{i+2,j+1} \\ e_{i+1,j-3} & e_{i+2,j-2} & e_{i+2,j-1} & e_{i+3,j} \end{bmatrix} = \begin{bmatrix} 1 & \frac{2}{3} & \frac{1}{3} & 0 \\ \frac{2}{3} & \frac{4}{9} & \frac{2}{9} & 0 \\ \frac{1}{3} & \frac{2}{9} & \frac{1}{9} & 0 \\ 0 & 0 & 0 & 0 \end{bmatrix},$$

$$\mathbf{E}_{I,J+1} = \begin{bmatrix} e_{i,j} & e_{i,j+1} & e_{i+1,j+2} & e_{i+1,j+3} \\ e_{i,j-1} & e_{i+1,j} & e_{i+1,j+1} & e_{i+2,j+2} \\ e_{i+1,j-2} & e_{i+1,j-1} & e_{i+2,j} & e_{i+2,j+1} \\ e_{i+1,j-3} & e_{i+2,j-2} & e_{i+2,j-1} & e_{i+3,j} \end{bmatrix}$$

$$= \begin{bmatrix} 0 & \frac{1}{3} & \frac{2}{3} & 1 \\ 0 & \frac{2}{9} & \frac{4}{9} & \frac{2}{3} \\ 0 & \frac{1}{9} & \frac{2}{9} & \frac{1}{3} \\ 0 & 0 & 0 & 0 \end{bmatrix},$$

$$\mathbf{E}_{I,J-1} = \begin{bmatrix} e_{i,j} & e_{i,j+1} & e_{i+1,j+2} & e_{i+1,j+3} \\ e_{i,j-1} & e_{i+1,j} & e_{i+1,j+1} & e_{i+2,j+2} \\ e_{i+1,j-2} & e_{i+1,j-1} & e_{i+2,j} & e_{i+2,j+1} \\ e_{i+1,j-3} & e_{i+2,j-2} & e_{i+2,j-1} & e_{i+3,j} \end{bmatrix}$$

$$= \begin{bmatrix} 0 & 0 & 0 & 0 \\ \frac{1}{3} & \frac{2}{9} & \frac{1}{9} & 0 \\ \frac{2}{3} & \frac{4}{9} & \frac{2}{9} & 0 \\ 1 & \frac{2}{3} & \frac{1}{3} & 0 \end{bmatrix}, \quad \text{and}$$

$$\mathbf{E}_{I+1,J+1} = \begin{bmatrix} e_{i,j} & e_{i,j+1} & e_{i+1,j+2} & e_{i+1,j+3} \\ e_{i,j-1} & e_{i+1,j} & e_{i+1,j+1} & e_{i+2,j+2} \\ e_{i+1,j-2} & e_{i+1,j-1} & e_{i+2,j} & e_{i+2,j+1} \\ e_{i+1,j-3} & e_{i+2,j-2} & e_{i+2,j-1} & e_{i+3,j} \end{bmatrix}$$

$$= \begin{bmatrix} 0 & 0 & 0 & 0 \\ 0 & \frac{1}{9} & \frac{2}{9} & \frac{1}{3} \\ 0 & \frac{2}{9} & \frac{4}{9} & \frac{2}{3} \\ 0 & \frac{1}{3} & \frac{2}{3} & 1 \end{bmatrix}$$

in HWRF implementation.

b. Nest-moving algorithm

The nest-moving algorithm defines how movable nests automatically follow TC motion in the model. There are several nest-moving algorithms in the latest HWRF model, and any one of them can be adopted for the HWRF-B. The intuitive algorithm is the centroid of mean sea level pressure (MSLP). At the end of every time step, the MSLP at the centroid of the domain was computed. When the MSLP center moves more than one grid point on the parent domain away from the nest domain center (equivalent to three nest grid points from the center of the nest domain), the nest domain moves to a new position, keeping the TC at the center of the nest domain. Before tracking the center, some filtering is performed to properly define the center in weak TCs or to remove spurious minima since the MSLP is artificially extrapolated down to sea level over topography. The nest motion will be terminated if the nest attempts to move off of the parent domain. At every nest movement the majority of the data are passed between domains before and after the grid motion. Interpolation and hydrostatic mass balancing are only applied in the region at the leading edge of the moving nest. The model is then integrated forward after this process is completed.

It should be noted that starting with 2012, the operational HWRF has evolved every year. In this publication, we only documented the basic algorithm used in HWRF. In 2013, a more robust nest-moving algorithm was introduced by applying GFDL's TC location-finding technique (Marchok 2002) in the operational HWRF model. The optimized algorithm improves the accuracy of defining the TC center, especially for weak TCs. A detailed explanation of the implementation of the new tracking algorithm for the HWRF modeling system is documented in the online scientific documentation.[A1]

REFERENCES

Bao, J.-W., S. G. Gopalakrishnan, S. A. Michelson, F. D. Marks, and M. T. Montgomery, 2012: Impact of physics representations in the HWRFx on simulated hurricane structure and pressure–wind relationships. *Mon. Wea. Rev.*, **140**, 3278–3299, doi:10.1175/MWR-D-11-00332.1.

Blake, E. S., T. B. Kimberlain, R. J. Berg, J. P. Cangialosi, and J. L. Beven II, 2013: Tropical Cyclone Report Hurricane Sandy (AL182012) 22–29 October 2012. NOAA, 157 pp. [Available online at http://www.nhc.noaa.gov/data/tcr/AL182012_Sandy.pdf.]

Brand, S., 1970: Interaction of binary cyclones of the western North Pacific Ocean. *J. Appl. Meteor.*, **9**, 433–441, doi:10.1175/1520-0450(1970)009<0433:IOBTCO>2.0.CO;2.

Fels, S. B., and M. D. Schwarzkopf, 1975: The simplified exchange approximation: A new method for radiative transfer calculations. *J. Atmos. Sci.*, **32**, 1475–1488, doi:10.1175/1520-0469(1975)032<1475:TSEAAN>2.0.CO;2.

Ferrier, B. S., 2005: An efficient mixed-phase cloud and precipitation scheme for use in operational NWP models. *Eos, Trans. Amer. Geophys. Union*, 86 (Joint Assembly Suppl.), Abstract A42A–02.

[A1] See footnote 1.

Fujiwhara, S., 1921: The mutual tendency towards symmetry of motion and its application as a principle in meteorology. *Quart. J. Roy. Meteor. Soc.*, **47**, 287–293, doi:10.1002/qj.49704720010.

Goldenberg, S. B., S. G. Gopalakrishnan, T. Quirino, F. Marks Jr., V. Tallapragada, S. Trahan, X. Zhang, and R. Atlas, 2015: The 2012 triply nested, high-resolution operational version of the Hurricane Weather Research and Forecasting System (HWRF): Track and intensity forecast verifications. *Wea. Forecasting*, **30**, 710–729, doi:10.1175/WAF-D-14-00098.1.

Gopalakrishnan, S. G., and Coauthors, 2002: An operational multiscale hurricane forecasting system. *Mon. Wea. Rev.*, **130**, 1830–1847, doi:10.1175/1520-0493(2002)130<1830:AOMHFS>2.0.CO;2.

——, N. Surgi, R. Tuleya, and Z. Janjić, 2006: NCEP's two-way-interactive-moving-nest NMM-WRF modeling system for hurricane forecasting. Preprints, *27th Conf. on Hurricanes and Tropical Meteorology*, Monterey, CA, Amer. Meteor. Soc., 7A.3. [Available online at http://ams.confex.com/ams/pdfpapers/107899.pdf.]

——, F. Marks, X. Zhang, J.-W. Bao, K.-S. Yeh, and R. Atlas, 2011: The experimental HWRF system: A study on the influence of horizontal resolution on the structure and intensity changes in tropical cyclones using an idealized framework. *Mon. Wea. Rev.*, **139**, 1762–1784, doi:10.1175/2010MWR3535.1.

——, S. Goldenberg, T. Quirino, X. Zhang, F. Marks, K.-S. Yeh, R. Atlas, and V. Tallapragada, 2012: Toward improving high-resolution numerical hurricane forecasting: Influence of model horizontal grid resolution, initialization, and physics. *Wea. Forecasting*, **27**, 647–666, doi:10.1175/WAF-D-11-00055.1.

——, F. Marks, J. A. Zhang, X. Zhang, J.-W. Bao, and V. Tallapragada, 2013: Study of the impacts of vertical diffusion on the structure and intensity of the tropical cyclones using the high-resolution HWRF system. *J. Atmos. Sci.*, **70**, 524–541, doi:10.1175/JAS-D-11-0340.1.

Haus, B., D. Jeong, M. A. Donelan, J. A. Zhang, and I. Savelyev, 2010: Relative rates of sea-air heat transfer and frictional drag in very high winds. *Geophys. Res. Lett.*, **37**, L07802, doi:10.1029/2009GL042206.

Hendricks, E. A., M. S. Peng, X. Ge, and T. Li, 2011: Performance of a dynamic initialization scheme in the Coupled Ocean–Atmosphere Mesoscale Prediction System for Tropical Cyclones (COAMPS-TC). *Wea. Forecasting*, **26**, 650–663, doi:10.1175/WAF-D-10-05051.1.

Hong, S.-Y., and H.-L. Pan, 1996: Nonlocal boundary layer vertical diffusion in a medium-range forecast model. *Mon. Wea. Rev.*, **124**, 2322–2339, doi:10.1175/1520-0493(1996)124<2322:NBLVDI>2.0.CO;2.

——, and ——, 1998: Convective trigger function for a mass flux cumulus parameterization scheme. *Mon. Wea. Rev.*, **126**, 2621–2639, doi:10.1175/1520-0493(1998)126<2599:CTFFAM>2.0.CO;2.

Hsiao, L.-F., D.-S. Chen, Y.-H. Kuo, Y.-R. Guo, T.-C. Yeh, J.-S. Hong, C.-T. Fong, and C.-S. Lee, 2012: Application of WRF 3DVAR to operational typhoon prediction in Taiwan: Impact of outer loop and partial cycling approaches. *Wea. Forecasting*, **27**, 1249–1263, doi:10.1175/WAF-D-11-00131.1.

Janjić, Z., J. Gerrity, and S. Nickovic, 2001: An alternative approach to nonhydrostatic modeling. *Mon. Wea. Rev.*, **129**, 1164–1178, doi:10.1175/1520-0493(2001)129<1164:AAATNM>2.0.CO;2.

Kurihara, Y., and R. E. Tuleya, 1974: Structure of a tropical cyclone developed in a three- dimensional numerical simulation model. *J. Atmos. Sci.*, **31**, 893–919, doi:10.1175/1520-0469(1974)031<0893:SOATCD>2.0.CO;2.

——, G. J. Tripoli, and M. A. Bender, 1979: Design of a movable nested-mesh primitive equation model. *Mon. Wea. Rev.*, **107**, 239–249, doi:10.1175/1520-0493(1979)107<0239:DOAMNM>2.0.CO;2.

——, R. E. Tuleya, and M. A. Bender, 1998: The GFDL Hurricane Prediction System and its performance in the 1995 hurricane season. *Mon. Wea. Rev.*, **126**, 1306–1322, doi:10.1175/1520-0493(1998)126<1306:TGHPSA>2.0.CO;2.

Lacis, A. A., and J. E. Hansen, 1974: A parameterization for the absorption of solar radiation in the earth's atmosphere. *J. Atmos. Sci.*, **31**, 118–133, doi:10.1175/1520-0469(1974)031<0118:APFTAO>2.0.CO;2.

Lander, M., and G. J. Holland, 1993: On the interaction of tropical-cyclone scale vortices. I: Observations. *Quart. J. Roy. Meteor. Soc.*, **119**, 1347–1361, doi:10.1002/qj.49711951406.

Liu, Y., D.-L. Zhang, and M. K. Yau, 1997: A multiscale numerical study of Hurricane Andrew (1992). Part I: Explicit simulation and verification. *Mon. Wea. Rev.*, **125**, 3073–3093, doi:10.1175/1520-0493(1997)125<3073:AMNSOH>2.0.CO;2.

Lorenz, E. N., 1969: Atmospheric predictability as revealed by naturally occurring analogues. *J. Atmos. Sci.*, **26**, 636–646, doi:10.1175/1520-0469(1969)26<636:APARBN>2.0.CO;2.

Marchok, T. P., 2002: How the NCEP tropical cyclone tracker works. Preprints, *25th Conf. on Hurricanes and Tropical Meteorology*, San Diego, CA, Amer. Meteor. Soc., P1.13. [Available online at https://ams.confex.com/ams/pdfpapers/37628.pdf.]

Michalakes, J., J. Dudhia, D. Gill, T. B. Henderson, J. Klemp, W. Skamarock, and W. Wang, 2004: The Weather Research and Forecast Model: Software architecture and performance. *Proc. 11th Workshop on the Use of High Performance Computing in Meteorology*, Reading, United Kingdom, ECMWF, 156–168, doi:10.1142/9789812701831_0012.

Montgomery, M. T., and Coauthors, 2012: The Pre-Depression Investigation of Cloud-Systems in the Tropics (PREDICT) experiment: Scientific basis, new analysis tools, and some first results. *Bull. Amer. Meteor. Soc.*, **93**, 153–172, doi:10.1175/BAMS-D-11-00046.1.

Ngodock, H. E., S. R. Smith, and G. A. Jacobs, 2007: Cycling the representer algorithm for variational data assimilation with the Lorenz attractor. *Mon. Wea. Rev.*, **135**, 373–386, doi:10.1175/MWR3281.1.

Pan, H.-L., and J. Wu, 1995: Implementing a mass flux convection parameterization package for the NMC medium-range forecast model. NMC Office Note 409, 40 pp. [Available online at http://www2.mmm.ucar.edu/wrf/users/phys_refs/CU_PHYS/Old_SAS.pdf.]

Pattanayak, S., U. C. Mohanty, and S. G. Gopalakrishnan, 2012: Simulation of very severe cyclone Mala over Bay of Bengal with HWRF modeling system. *Nat. Hazards*, **63**, 1413–1437, doi:10.1007/s11069-011-9863-z.

Quirino, T. S., J. Delgado, and X. Zhang, 2014: Improving the scalability of a hurricane forecast system in mixed-parallel environments: Advancing the WRF framework toward faster and more accurate forecasts. *Proc. 16th Int. Conf. on High Performance Computing and Communications*, Paris, France, IEEE, doi:10.1109/HPCC.2014.50.

Schwarzkopf, M. D., and S. Fels, 1991: The simplified exchange method revisited: An accurate, rapid method for computation of infrared cooling rates and fluxes. *J. Geophys. Res.*, **96**, 9075–9096, doi:10.1029/89JD01598.

Shen, B.-W., M. DeMaria, J.-L. F. Li, and S. Cheung, 2013: Genesis of Hurricane Sandy (2012) simulated with a global mesoscale model. *Geophys. Res. Lett.*, **40**, 4944–4950, doi:10.1002/grl.50934.

Sirutis, J. J., and K. Miyakoda, 1990: Subgrid scale physics in 1-month forecasts. Part I: Experiment with four parameterization packages. *Mon. Wea. Rev.*, **118**, 1043–1064, doi:10.1175/1520-0493(1990)118<1043:SSPIMF>2.0.CO;2.

Tallapragada, V., C. Kieu, Y. Kwon, S. Trahan, Q. Liu, Z. Zhang, and I.-H. Kwon, 2014: Evaluation of storm structure from the operational HWRF during 2012 implementation. *Mon. Wea. Rev.*, **142**, 4308–4325, doi:10.1175/MWR-D-13-00010.1.

Wang, Y., 1995: On an inverse balance equation in sigma coordinates for model initialization. *Mon. Wea. Rev.*, **123**, 482–488, doi:10.1175/1520-0493(1995)123<0482:AIBEIS>2.0.CO;2.

——, 2001: An explicit simulation of tropical cyclones with a triply nested movable mesh primitive equation model: TCM3. Part I: Model description and control experiment. *Mon. Wea. Rev.*, **129**, 1370–1394, doi:10.1175/1520-0493(2001)129<1370:AESOTC>2.0.CO;2.

Xu, H., X. Zhang, and X. Xu, 2013: Impact of Tropical Storm Bopha on the intensity change of Supertyphoon Saomai in the 2006 typhoon season. *Adv. Meteor.*, **2013**, 487010, doi:10.1155/2013/487010.

Yablonsky, R. M., and I. Ginis, 2013: Impact of a warm ocean eddy's circulation on hurricane-induced sea surface cooling with implications for hurricane intensity. *Mon. Wea. Rev.*, **141**, 997–1021, doi:10.1175/MWR-D-12-00248.1.

Yeh, K.-S., X. Zhang, S. G. Gopalakrishnan, S. Aberson, R. Rogers, F. D. Marks, and R. Atlas, 2012: Performance of the experimental HWRF in the 2008 hurricane season. *Nat. Hazards*, **63**, 1439–1449, doi:10.1007/s11069-011-9787-7.

Zhang, J. A., P. G. Black, J. R. French, and W. M. Drennan, 2008: First direct measurements of enthalpy flux in the hurricane boundary layer: The CBLAST results. *Geophys. Res. Lett.*, **35**, L14813, doi:10.1029/2008GL034374.

——, F. D. Marks, M. T. Montgomery, and S. Lorsolo, 2011a: An estimation of turbulent characteristics in the low-level region of intense Hurricanes Allen (1980) and Hugo (1989). *Mon. Wea. Rev.*, **139**, 1447–1462, doi:10.1175/2010MWR3435.1.

——, R. F. Rogers, D. S. Nolan, and F. D. Marks Jr., 2011b: On the characteristic height scales of the hurricane boundary layer. *Mon. Wea. Rev.*, **139**, 2523–2535, doi:10.1175/MWR-D-10-05017.1.

Zhang, X., T. Quirino, K.-S. Yeh, S. Gopalakrishnan, F. Marks, S. Goldenberg, and S. Aberson, 2011: HWRFx: Improving hurricane forecasts with high-resolution modeling. *Comput. Sci. Eng.*, **13**, 13–21, doi:10.1109/MCSE.2010.121.

Zhao, Y., B. Wang, and Y. Wang, 2007: Initialization and simulation of a landfalling typhoon using a variational bogus mapped data assimilation (BMDA). *Meteor. Atmos. Phys.*, **98**, 269–282, doi:10.1007/s00703-007-0265-4.